Structural geometry, fracture process zone and fracture energy

V. Veselý, L. Řoutil & Z. Keršner
Institute of Structural Mechanics, Faculty of Civil Engineering, Brno University of Technology, Czech Republic

ABSTRACT: This paper is focused on the influence of structural size and geometry on the size and shape of the fracture process zone (FPZ), and consequently on the progress of the fracture energy dissipated within the FPZ during the fracture process in structures made of quasi-brittle materials. The effect of structural geometry on its fracture behaviour is described here by two-parameter fracture mechanics, in particular by the constraint of stress near the equivalent elastic crack tip. The local fracture energy concept is evolved. Attention is paid to finding the intermediate stage of the fracture when there is no direct influence of the specimen boundary on the FPZ size and shape (and consequently the value of fracture energy dissipated within it). The research was conducted by means of numerical simulations of fracture tests in two testing configurations with different constraint conditions. The features of the distribution of local/averaged fracture energy along the specimen ligament are discussed. Based on the courses of these functions, it is shown that the size and shape of the FPZ are strongly influenced by structural size and geometry.

1 INTRODUCTION

Tensile failure of quasi-brittle materials like concrete typically starts with the development of a zone of inelastic material behaviour at a point within a structure with the strongest stress concentration. In this fracture process zone (FPZ) the material failure takes place via many mechanisms on many levels of the material structure. During failure propagation the FPZ changes its location within the structure, and therefore also its shape and size, and an opened stress-free crack remains behind it. Since the size of the FPZ is large in comparison to the usual dimensions of structural members, a nonlinear theory covering the energy dissipation of fracture mechanisms in the FPZ must be employed in the structural analysis, design and assessment of structures made of quasi-brittle materials.

Cohesive crack models are those most widely used and are relatively the simplest ones which are able to include the energy dissipation phenomena of concrete fracture. The efficient and reliable employment of these models within the structural analysis depends on successful tuning of the material model using appropriate material parameters. Although the experimental techniques for the determination of these characteristics are simple in principle, their direct application to the material model is usually incorrect due to the influence of specimen size and geometry on the gained material property.

The determination of the parameters of cohesive crack models has been refined in several aspects over the last two decades. The main effort was devoted to the determination of "true" fracture energy G_F, i.e. the value of fracture energy independent of the size and geometry of the specimen (Duan et al. 2002, 2003a,b, Karihaloo et al. 2003). Such methods are being developed to eliminate the main drawbacks of the direct application of the "work-of-fracture method", recommended by RILEM (1985), which is usually used for the determination of fracture energy G_F as the essential parameter of the cohesive crack models. The crucial disadvantage of the RILEM method is, as was already mentioned, the dependence of the determined fracture energy on the specimen size and geometry, and moreover, within one geometry the value decreases with decreasing ligament length.

The RILEM fracture energy therefore cannot be generally regarded as the material property G_F. Let us denote it as G_f for this moment. The dependence of G_f on specimen geometry and size is caused by the change in the size and shape of the FPZ during fracture propagation, which causes a change in the amount of energy dissipated in the zone. This alteration is prescribed by the location and distance of the FPZ in relation to the free surfaces of the body. The energy dissipated in the FPZ corresponding to certain size, geometry and boundary conditions of the structure is known as the local fracture energy g_f

(Hu & Wittmann 1992). Its distribution along ligaments is not constant, which is the reason for the non-uniform distribution of fracture energy G_f along the ligament, as reported e.g. by Hu & Wittmann (1992, 2000), Trunk & Wittmann (2001), Duan et al. (2002, 2003a,b), and Hu & Duan (2004).

The most considerable change in the local fracture energy g_f is close to the beginning and the end of the entire fracture process through the specimen ligament. In the beginning the FPZ develops, its size grows and is influenced (limited), as well as its shape, by the front free surface of the specimen (Hu & Wittmann 2000). Therefore, the amount of energy dissipated in the FPZ is lower at the beginning of the fracture than the average value of g_f dissipated farther in the material where the FPZ is not directly influenced by the specimen's boundaries. It is also well understood that the value of g_f decreases again when the FPZ approaches the back free surface of the specimen, because the size of the FPZ decreases. Also for this phenomenon an appropiate model was developed; the distribution of the local fracture energy along the specimen ligament is modelled by a bi-linear function (e.g. Duan et al. 2002, 2003a,b, Hu & Duan 2004). However, the characteristics of the transitional point, from which the decrease of g_f starts are described by the model rather schematically. Moreover, the utility of this model has only been demonstrated on geometries where the fracture process ends in a region of high constraint of stress (three-point bending and wedge splitting specimens – Duan et al. 2002, 2003a, Karihaloo et al. 2003). This paper tries to answer the question of whether and how much the location of the transitional point is dependent on specimen geometry and size.

The intermediate stage in the fracture process (in cases when the structure is large enough) is least influenced by the boundaries of the structure; therefore this part should be exploited for the evaluation of the true fracture energy, as proposed by Bažant (1996). It is usually assumed that in this stage of the fracture process the FPZ size is more or less constant and characteristic of the material. However, generally even in the intermediate stage the change in the size and shape of the FPZ may be considerable. The alteration of the FPZ in this stage is influenced by the stress distribution through the structure rather than directly by its free surfaces (boundary effect). Nevertheless, the stress distribution within the structure is, of course, affected by the structural geometry. This phenomenon is another topic of this proposed paper.

This paper is focused on the influence of structural size and the characteristics of stress constraint at the crack tip (which is a consequence of structural geometry) on the size and shape of the FPZ, and consequently on the variation of the local fracture energy g_f dissipated within the FPZ during the fracture process in structures/specimens made of quasi-brittle materials. Attention is paid in particular to finding the intermediate stage of the fracture when there is no direct influence on the FPZ size and shape (and consequently the value of g_f) from the specimen's boundaries. The research was conducted by means of the analyses of fracture test simulations in two testing configurations with different constraint conditions.

2 FRACTURE ENERGY CONCEPT

Fracture energy is defined as the energy needed to create a crack surface of unit area. According to the "work-of-fracture method" (RILEM 1985), the fracture energy is calculated as the area under the whole load vs. load-point-displacement curve (P–d diagram) recorded during the fracture test (possibly extrapolated to the space for larger displacement than measured) and divided by the area of the initial specimen ligament. For a specimen of width W, breadth B, with an initial crack of length a_0, the fracture energy is calculated as

$$G_f = \frac{1}{(W - a_0)B} \int P \,\mathrm{d}d\,. \tag{1}$$

This method is based on the cohesive crack model approach (for concrete fictitious crack model by Hillerborg et al. 1976).

2.1 *Non-constant fracture energy distribution*

The fracture energy G_f determined according to the RILEM method depends, within one geometry, on the relative notch depth $\alpha_0 = a_0/W$, as was discovered in many experiments and summarized by Karihaloo et al. (2003). The non-constant distribution of the local fracture energy g_f along the specimen ligament is the reason for this phenomenon. Since the courses of $G_f(\alpha)$ from these published experiments are only monotonously decreasing, a bilinear model for the distribution of g_f along a specimen ligament was proposed (Duan et al. 2002, 2003a,b). This model approximates the dependence of g_f vs. the initial ligament length $W - a$ wia a bilinear function governed by two parameters: the "true" fracture energy G_F and a transitional ligament length a_l^*. At sufficient distance from the specimen's free surface, the value of fracture energy is constant and can be regarded as the material property G_F. From a specific point, whose distance to the specimen's back face is equal to a_l^*, the value of the fracture energy decreases and at the back face it is zero. As a consequence, a simple method for the determination of the "true" fracture energy from a low number of tests was derived (Karihaloo et al. 2003). The value of G_F determined by this method is reported to be, at least within one geometry, independent of the relative notch depth α_0.

Let us note that the bilinear fracture energy distribution model and subsequently the simple method for the determination of the "true" specific fracture energy has been introduced only for three-point bending (SEN-TPB) and wedge splitting testing configurations which are characterized by high constraint (in case of SEN-TPB only for longer cracks, see Fig. 3).

2.2 *Local fracture energy*

The local fracture energy g_f is the specific energy which dissipates in a FPZ of an actual size and shape that corresponds to the size, shape and boundary conditions of the specimen at a certain time point in the fracture process. The distribution of this quantity along the specimen ligament is generally far from constant. As was noted above, its value is influenced considerably by the relation of the boundaries of the FPZ to the specimen's boundaries.

The energy dissipated from the beginning of the fracture process to its certain step i can be calculated as

$$W_{f,i} = \int_0^{d_i} P \,\mathrm{d}d - \frac{1}{2} P_i^2 C_i \,, \tag{2}$$

where $P =$ load, $d =$ load-point-displacement and $C = d/P =$ specimen compliance. W_f is referred to as a work of fracture. For fracture energy it is true that:

$$G_{f,i} = \frac{1}{\Delta a_i B} W_{f,i} \,, \tag{3}$$

where $\Delta a_i = a_i - a_0 =$ equivalent elastic crack extension at time point i. As is obvious from Eq. 3, the fracture energy $G_{f,i}$ is an averaged value of the instantaneous specific work of fracture dissipated from the beginning of fracture to its i-th step. The RILEM G_f is the averaged fracture energy of the fracture process through the entire specimen ligament.

In contrast, the local fracture energy is a specific work of fracture dissipated between two close-together steps of the fracture process:

$$g_{f,i} = \frac{1}{(\Delta a_i - \Delta a_{i-1}) B} (W_{f,i} - W_{f,i-1}) \,. \tag{4}$$

The mutual relation between the calculation of $G_{f,i}$ and $g_{f,i}$ is illustrated in Fig. 1.

Note that at each point in the fracture process, the value of g_f is equal to the value of the fracture resistance $\mathcal{R}$ calculated as $\mathcal{R} = K_I^e / E$, where $K_I^e =$ the stress intensity factor at an equivalent elastic crack tip.

3 FRACTURE PROCESS ZONE AND CRACK TIP STRESS FIELD

The effect of the size and geometry of the testing specimen on the value of the determined fracture energy G_f is a consequence of the change in the local fracture energy g_f during the fracture process. The reason for the phenomenon most probably consists in the change in the shape and size of the FPZ ahead of the tip of the progressing macroscopic crack.

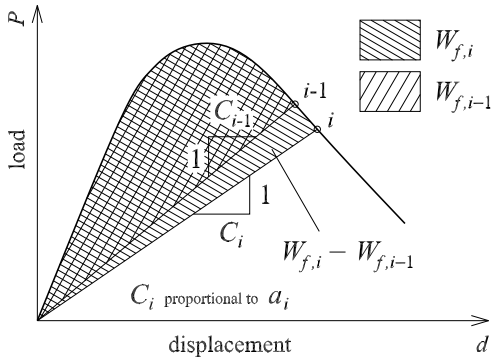

Figure 1: Calculation of work of fracture from a load–displacement diagram

The relationship between the fracture behaviour of a pre-cracked body and its geometry can be described by means of two-parameter fracture mechanics based on the power series expression of the crack tip stress field which was introduced by Williams (1957). For the stress tensor it is true that:

$$\sigma_{ij} = \sum_{n=1}^{\infty} \left(A_n \frac{n}{2} \right) r^{\frac{n}{2}-1} f_{ij}(n, \theta) \,, \tag{5}$$

where $A_n =$ coefficients, $f_{ij} =$ known functions and r, $\theta =$ polar coordinates. Two-parameter linear elastic fracture mechanics (LEFM) deals with the first two terms of the series; the singular one which is appropriate to the stress intensity factor K_I of classical fracture mechanics, and the constant one corresponding with the T-stress:

$$\sigma_{ij} = \frac{K_I}{\sqrt{2\pi r}} f_{ij}(\theta) + T \delta_{1i} \delta_{1j} \,, \tag{6}$$

where $\delta_{kl} =$ Cronecker delta.

In brittle and elasto-plastic materials, the size and shape of an inelastic zone ahead of a crack tip is generally governed by the stress multiaxiality at the crack tip. The multiaxiality differs for different geometries and is the reason for the so-called constraint effect, i.e. pre-cracked bodies with different geometries might exhibit considerably different fracture behaviour, even if they are characterized by the same stress intensity factor. For an explanation of the constraint effect not only singular but also higher order terms of the Williams' series must be taken into account. The T-stress is employed as a crucial component in this theory because it can serve as a measure of the stress constraint near the crack tip. When the constraint is low (T negative), the inelastic zone is relatively large and is oriented in the direction of the crack

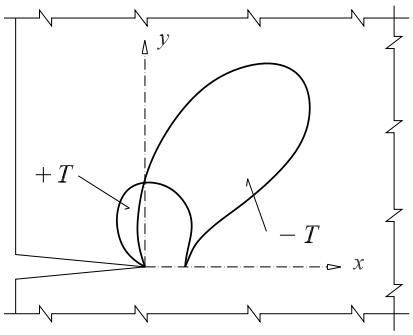

Figure 2: Shapes of plastic zone for different constraint conditions

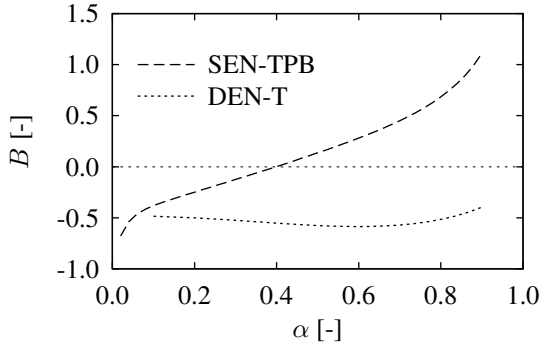

Figure 3: Plot of $B(\alpha)$ function for SEN-TPB and DEN-T testing configurations

growth, while in contrast, for high constraint (T positive) the inelastic zone is smaller (constrained) and it is set in the opposite direction (see Fig. 2). Equivalently to the T-stress a dimensionless biaxiality factor B can be used for characterizing the constraint effect as $B = T\sqrt{\pi a}/K_I$ (Leevers & Radon 1982).

The straightforward application of the two-parameter LEFM in the field of quasi-brittle materials is not possible, since no single sharp crack and plastic zone ahead of its tip exists in these materials. Failure mechanisms characteristic of the FPZ in quasi-brittle materials differ substantially from failure mechanisms appropriate to brittle and ductile materials, which implies significant differences between the shapes of nonlinear zones in these mentioned materials. However, the relation of local fracture energy to the parameters that enable a more accurate description of the stress field near the macroscopic crack may be useful within the explanation of the effect of specimen geometry and size on local fracture energy. Two-parameter LEFM tools have already been employed in connection with the equivalent elastic and/or cohesive crack approach for capturing the effect of structural geometry on the R-curve shape (Veselý & Keršner 2004, 2006).

4 NUMERICAL ANALYSES OF FRACTURE TESTS

4.1 *Goal and description of the analyses*

The progress of both local and averaged fracture energy during the fracture process through the specimen ligament is studied in this section. The possible influence of specimen size and geometry on both expressions of the fracture energy is investigated.

Two testing configurations were chosen for the study as representatives of two different types of stress constraint at the crack tip: single edge notched beam under three point bending (SEN-TPB – Fig. 4) and double edge notched panel under tension (DEN-T – Fig. 5). While DEN-T is characterized by low constraint in the entire domain of the definition of α, the constraint is rather high in the case of SEN-TPB, especially for long cracks. The plot of B against α is displayed in Fig. 3 (data from Knésl & Bednář 1998).

For each geometry, five sizes (depths of specimens: W for SEN-TPB and $2W$ for DEN-T) were considered: 80, 160, 320, 640, and 1280 mm. Only the middle and both outside sizes are present in the proposed paper. Breadth b of all sizes and both geometries was equal to 80 mm. Other dimensions of the specimens can be derived from schemes on Fig. 4 and 5. Five notch lengths α_0 for each specimen size were taken into account: 0.1, 0.3, 0.5, 0.7, and 0.85.

The discussed fracture tests were performed virtually as numerical simulations using the commercial FEM package ATENA (Červenka et al. 2003). The analyses were conducted in a plain stress state with a fracture–plastic constitutive model. The fracture model is based on the classical orthotropic smeared crack formulation and crack band model, and it employs the Rankine failure criterion and exponential softening (Červenka et al. 2003). The parameters of the material model were generated by the software for the input cubic compressive strength of concrete $f_{cu} = 61$ MPa. The most important parameters of the fracture model that influence fracture behaviour are tensile strength $f_t = 3.719$ MPa, fracture energy $G_F^{FEM} = 92.98$ Jm^{-2} and an exponential type of softening traction–separation law with the crack opening at the complete release of stress $w_c = 0.1285$ mm.

4.2 *Results and evaluation of fracture energy*

Load–displacement diagrams from numerical simulations are displayed in graphs a), b), and c) on Fig. 4 and Fig. 5 for the SEN-TPB and DEN-T testing configuration, respectively. Descending branches of the P–d diagram predicted using LEFM from G_F^{FEM} used in numerical simulations are plotted in the graphs as well (dotted line, labelled as LEFM).

Fracture energy was determined from the P–d diagrams. For each P–d diagram, the following quantities were calculated:

(i) Averaged fracture energy G_f for the very last point of the curve was calculated from Eq. 3, where

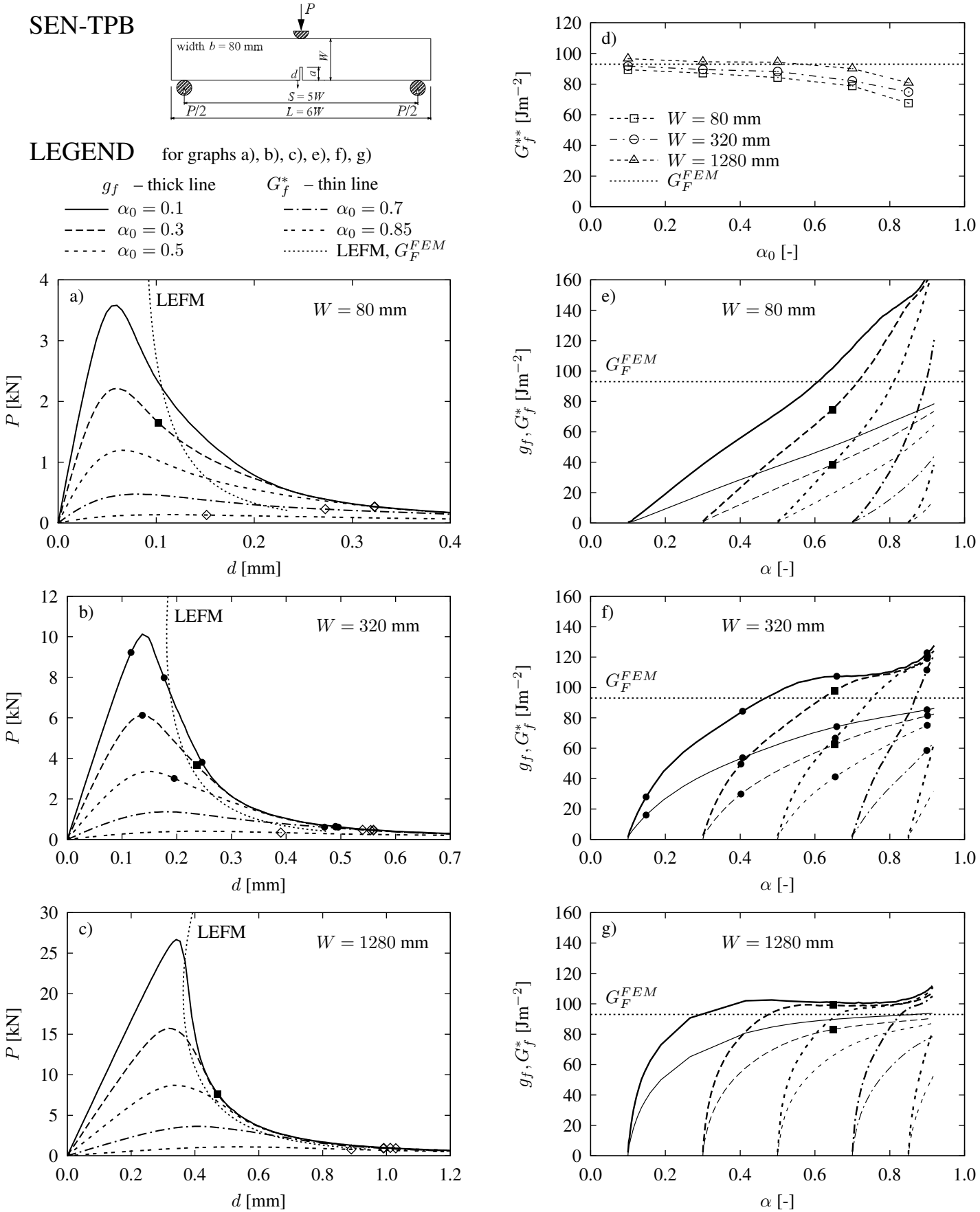

Figure 4: SEN-TPB testing configuration: Load–deflection diagrams from numerical simulations for considered specimen sizes W and relative notch lengths α_0 (graphs a), b), and c)) and appropriate courses of local fracture energy g_f and average fracture energy G_f^* as functions of relative effective crack length α (graphs e), f), and g)). Values of fracture energy G_f^{**} for different sizes and relative notch lengths (graph d)).

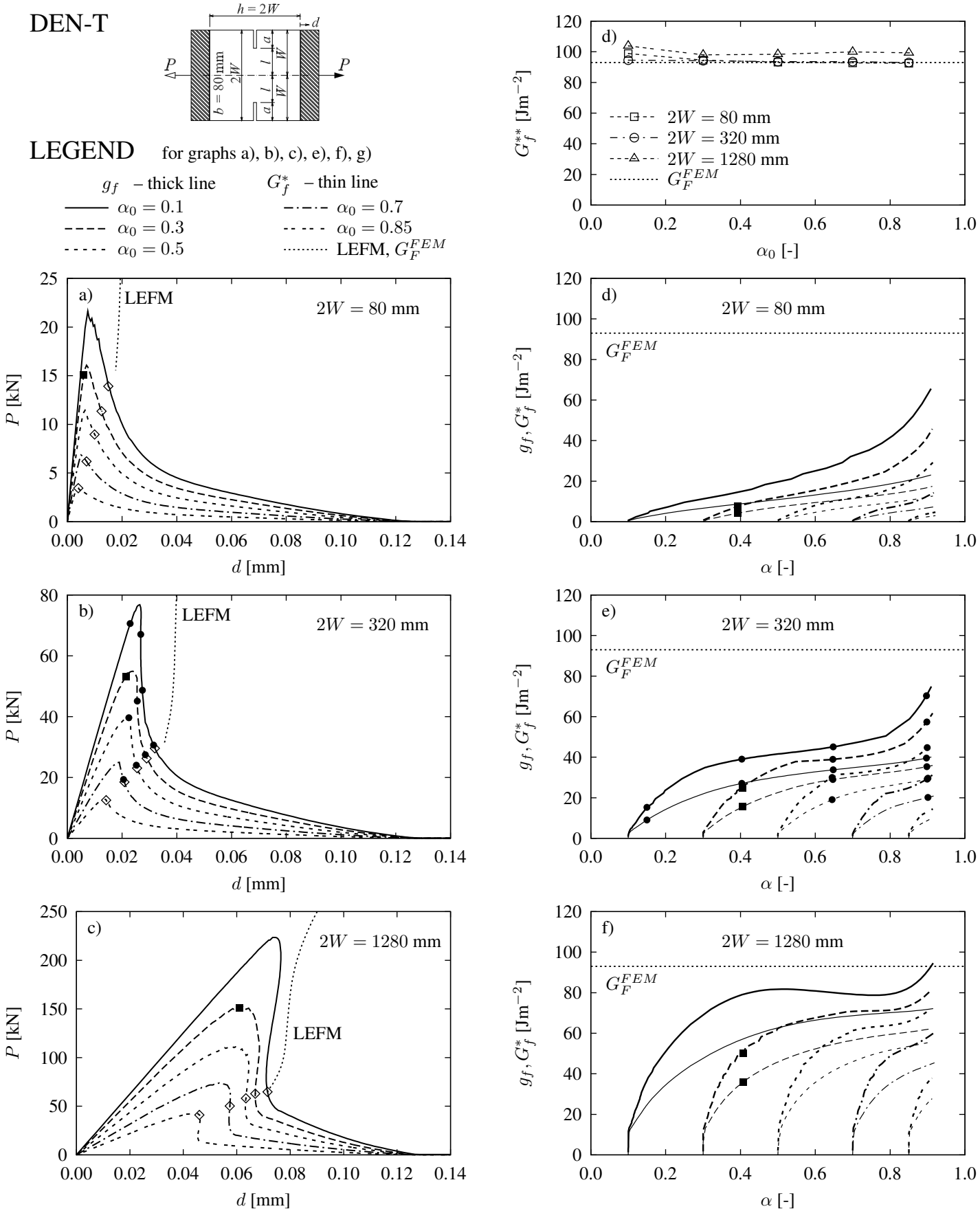

Figure 5: DEN-T testing configuration: Load–displacement diagrams from numerical simulations for considered specimen sizes $2W$ and relative notch lengths α_0 (graphs a), b), and c)) and appropriate courses of local fracture energy g_f and average fracture energy G_f^* as functions of relative effective crack length α (graphs e), f), and g)). Values of fracture energy G_f^{**} for different sizes and relative notch lengths (graph d)).

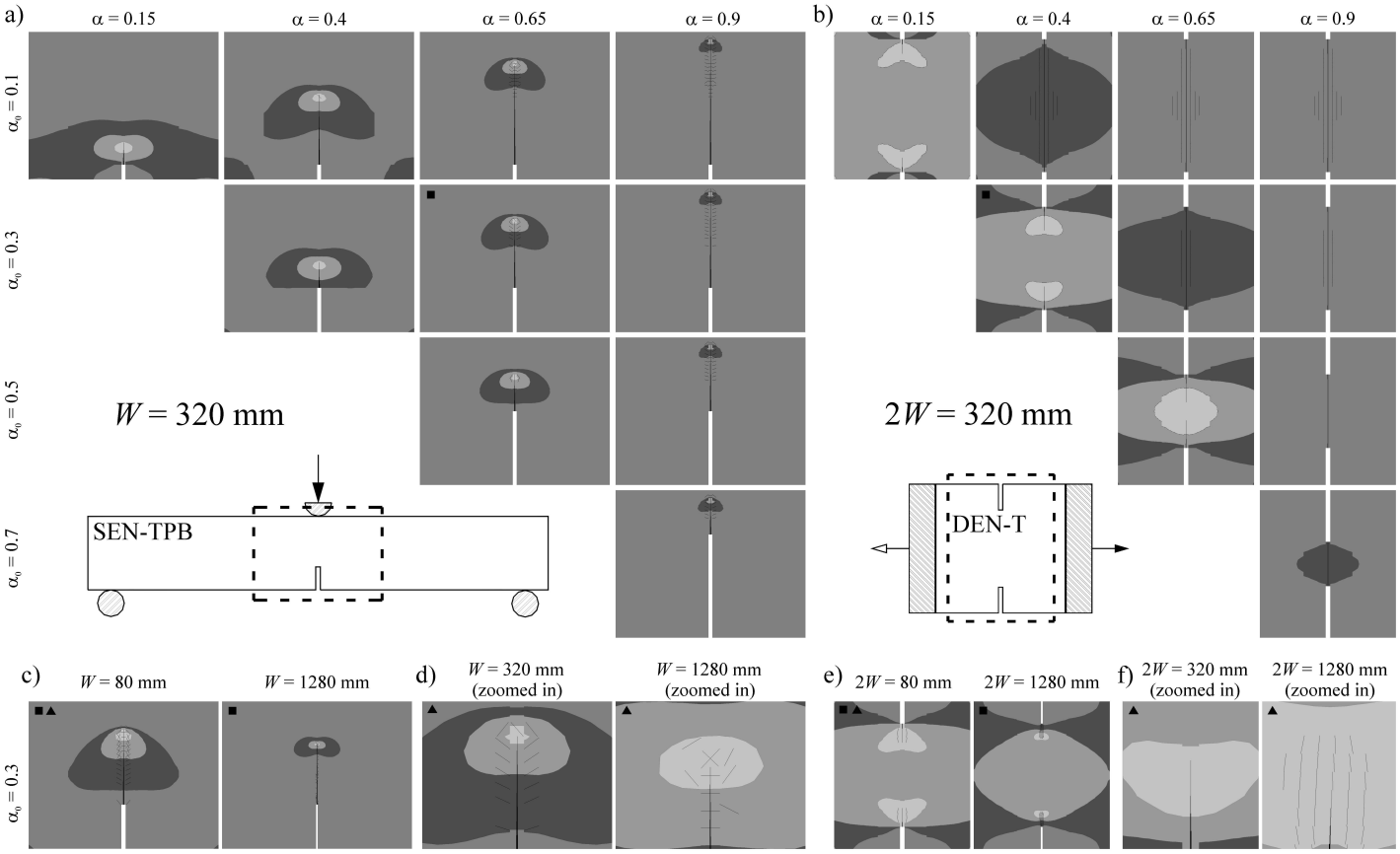

Figure 6: Crack opening stress profiles – SEN-TPB (left) and DEN-T testing configurations

Δa was assumed equal to $W - a$ (the ligament is completely broken). It is the same value as the RILEM G_f using Eq. 1. This fracture energy is denoted G_f^{**} and the values for individual relative notch lengths and individual sizes are plotted in graphs d) on Fig. 4 and Fig. 5 for SEN-TPB and DEN-T, respectively.

(ii) Averaged fracture energy G_f for each point of the curve was calculated from Eq. 3, where equivalent elastic crack extension Δa at the point was determined from the secant specimen compliance according to the effective crack model (Nallathambi & Karihaloo 1986). This fracture energy is denoted here as G_f^*. Since the function of geometry used in the procedure of calculating Δa is limited (in this case by $\alpha = 0.92$ for both considered geometries), the courses of the $G_f^*(\alpha)$ functions plotted in graphs d), e), and f) on Fig. 4 and Fig. 5 end at a point of fracture process, where the unbroken ligament is formed by 8 % of the specimen depth. The points which correspond to the end points of the $G_f^*(\alpha)$ functions are marked in the appropriate P–d diagram by the empty diamond sign.

(iii) Local fracture energy g_f for each point in the curve was calculated from Eq. 4. The equivalent elastic crack extension Δa was assumed to be the same as in item (ii). The courses of the $g_f(\alpha)$ functions are plotted also in graphs d), e), and f) on Fig. 4 and Fig. 5. The course of G_F^{FEM} is also displayed in these graphs (horizontal dotted line).

4.3 *Opening stress profiles*

The stress field within the specimens during the test was analyzed. The profiles of the crack opening stress σ at particular steps of the fracture process are displayed in Fig. 6 for the SEN-TPB (left) and DEN-T (right) testing configuration, respectively. The progress of the shape of iso-areas of the crack opening stress can be illustrated by the sequence of shots. The shots are created for the specimens with the relative notch lengths $\alpha_0 = 0.1, 0.3, 0.5$, and 0.7 (from top to bottom) at stages in the fracture process appropriate to the actual relative equivalent elastic crack $\alpha =$ 0.15, 0.4, 0.65 and 0.9 (from left to right). Points appropriate to these stages are emphasized on the curves in graphs b) and e) in Fig. 4 and Fig. 5 by black circles. There are three contour iso-stress areas depicted on the shots: dark grey ($\sigma \in (1, 2)$ MPa), middle grey ($\sigma \in (2, 3)$ MPa), and light grey ($\sigma > 3$ MPa). Note that the tensile strength of the concrete used in the simulations was equal to $f_t = 3.719$ MPa.

Sections a) and b) of Fig. 6 correspond to the middle size of the specimens. For the other specimen sizes the evolution of the iso-stress contour shape remains similar contrariwise to its size. Section c) of Fig. 6 compares the two outside SEN-TPB specimen sizes with the chosen $\alpha_0 = 0.3$ at the selected stage of frac-

ture ($\alpha = 0.65$) with an appropriate case for the middle size. The compared shots of sections a) and c) are marked by black squares, similar to the points appropriate to these stages on curves in graphs a), b) and c) on Fig. 4. In section d) of Fig. 6, the crack tip regions of both the middle and the largest size are zoomed in in such a way that the scale of the shots remains equal to the shot of the smallest specimen size (section c) left). The appropriate shots of Fig. 6 compared in the section d) are marked by black triangles. These comparisons are similarly performed in sections b), e) and f) for the DEN-T configuration; an example with $\alpha_0 = 0.3$ and $\alpha = 0.4$ is displayed.

5 CONCLUSIONS

The following conclusions were obtained from the present numerical study:

(i) The size and shape of the FPZ of fractured quasi-brittle materials are strongly influenced by the size of specimen and its structural geometry. The parameter of the constraint of stress at the equivalent elastic crack tip can be employed to characterize this effect.

(ii) The values of the fracture energy averaged over the entire ligament (RILEM definition) correspond to the value of the fracture energy used as the input in the simulations. A slight decrease in "RILEM" fracture energy is only observed in the case of SEN-TPB geometry for increasing α_0.

(iii) Local fracture energy approaches the value of the fracture energy used in the simulations for very large specimens only. It is evident that for a high/low constraint this value is reached from above/below. An intermediate stage in the fracture process exploitable for the evaluation of the true fracture energy was found only for the largest size of SEN-TPB specimens with short notches.

(iv) Both considered geometries are substantially different from the crack tip stress constraint point of view. From the crack opening stress profiles depicted, it is possible to suppose the FPZ is constrained in size when approaching the high stress constraint area (SEN-TPB for $\alpha > 0.5$). Low constraint of FPZ size is evident in the case of DEN-T geometry or for SEN-TPB with very short cracks ($\alpha < 0.2$).

The conclusions of this research will be investigated using other geometries covering an even larger range of stress constraint near the crack tip than was presented in this study.

ACKNOWLEDGEMENT

This outcome has been achieved with the financial support of the Ministry of Education, Youth and Sports, project No. 1M0579 – CIDEAS research centre. In this undertaking, theoretical results gained in the project Grant Agency of Czech Republic 103/07/P403 were partially exploited.

REFERENCES

Bažant, Z.P. 1996. Analysis of work-of-fracture method for measuring fracture energy of concrete. *Journal of Engineering mechanics*, 122(2): 138–144.

Červenka, V. et al. 2003. *ATENA Program Documentation, Theory manual*. Prague: Cervenka Consulting.

Duan, K., Hu, X.-Z. & Wittmann, F.H. 2002. Explanation of size effect in concrete fracture using non-uniform energy distribution. *Mater. Struct.*, 35: 326–331.

Duan, K., Hu, X.-Z. & Wittmann, F.H. 2003a. Boundary effect on concrete fracture and non-constant fracture energy distribution. *Eng. Fract. Mech.*, 70: 2257–2268.

Duan, K., Hu, X.-Z. & Wittmann, F.H. 2003b. Thickness effect on fracture energy of cementitious materials. *Cem. Concr. Res.*, 33: 499–507.

Hillerborg, A., Modéer, M. & Petersson, P-E. 1976. Analysis of crack formation and crack growth in concrete by means of fracture mechanics and finite elements. *Cem. Concr. Res.*, 6: 773–782.

Hu, X.-Z. & Duan, K. 2004. Influence of fracture process zone height on fracture energy of concrete. *Cem. Concr. Res.*, 34: 1321–1330.

Hu, X.-Z. & Wittmann, F.H. 1992. Fracture energy and fracture process zone. *Mater. Struct.*, 25: 319–326.

Hu, X.-Z. & Wittmann, F.H. 2000. Size effect on toughness induced by crack close to free surface. *Eng. Fract. Mech.*, 65: 209–221.

Karihaloo, B. L., Abdalla, H. M. & Imjai, T. 2003. A simple method for determining the true specific fracture energy of concrete. *Mag. Concr. Res.*, 55: 471–481.

Knésl, Z. & Bednář, K. 1998. *Two-parameter fracture mechanics: Calculation of parameters and their values* (in Czech). Brno: Institute of Physics of Materials, Czech Academy of Sciences.

Leevers, P.S. & Radon, J.S. 1982. Inherent stress biaxiality in various fracture specimen geometries. *Int. J. Fract.*, 19: 311–325.

Nallathambi, P. & Karihaloo, B. L. 1986. Determination of specimen-size independent fracture toughness of plain concrete. *Mag. Concr. Res.*, 38: 67–76.

RILEM Committee FMC 50 (Recommendation) 1985. Determination of the fracture energy of mortar and concrete by means of three-point bend test on notched beams. *Mater. Struct.*, 18: 285–290.

Trunk, B. & Wittmann, F.H. 2001. Influence of size on fracture energy of concrete. *Mater. Struct.*, 34: 260–265.

Veselý, V. & Keršner, Z. 2004. Resistance surface concept for concrete fracture. In V. C. Li, K. J. Willam, C. K. Y. Leung, & S. L. Billington, eds., *Fracture Mechanics of Concrete and Concrete Structures; Proc. of 5th Int. Conf. FraMCoS, Vail, USA, 2004*, 1: 189–196. IaFraMCos.

Veselý, V. & Keršner, Z. 2006. R-curves from equivalent elastic crack approach: effect of structural geometry on fracture behaviour. In A.M. Brandt, V.C. Li, & I.H. Marshall, eds, *Brittle Matrix Composites 8; Proc. Int. Symp. BMC8, Warsaw, Poland, 2006*, 527–536. Cambridge: Woodhead Publishing Limited.

Williams, M.L. 1957. On the stress distribution at the base of stationary crack. *ASME J. Appl. Mech.*, 24: 109–114.